JOURNAL OF PETROLOGY | VOLUME 54 | NUMBER 3 | PAGES 525–537 | 2013 | doi:10.1093/petrology/egs076

Dy/Dy*: Variations Arising from Mantle Sources and Petrogenetic Processes

JON DAVIDSON[1]*, SIMON TURNER[2] AND TERRY PLANK[3]

[1]DEPARTMENT OF EARTH SCIENCES, DURHAM UNIVERSITY, DURHAM DH1 3LE, UK

[2]DEPARTMENT OF EARTH AND PLANETARY SCIENCES, MACQUARIE UNIVERSITY, SYDNEY, NSW 2109, AUSTRALIA

[3]DEPARTMENT OF EARTH AND ENVIRONMENTAL SCIENCES, COLUMBIA UNIVERSITY, LAMONT–DOHERTY EARTH OBSERVATORY, PO BOX 1000, 61 RTE 9 W, PALISADES, NY 10964, USA

RECEIVED SEPTEMBER 13, 2012; ACCEPTED SEPTEMBER 20, 2012
ADVANCE ACCESS PUBLICATION NOVEMBER 19, 2012

Dy/Dy is the measured value of Dy, a representative middle rare earth element (REE), compared with the value interpolated between La and Yb on a REE plot. It is essentially a measure of the 'concavity' of a REE pattern. The use of Dy/Dy* as a proxy for REE pattern shape allows us to compare large amounts of REE data, which can be difficult using standard REE patterns. When Dy/Dy* is combined with Dy/Yb (the slope of the middle-to-heavy REE pattern) REE patterns can effectively be classified by shape. We present a new set of high-quality REE (and other trace element) data for young volcanic rocks from six arcs. When plotted on the Dy/Dy*–Dy/Yb diagram they define a broad negative correlation from LREE-depleted (Tonga–Kermadec) to LREE-enriched (Philippines and Indonesia). This trend corresponds to decreasing Dy/Dy*, reflecting REE patterns varying from concave-down to concave-up respectively. When cogenetic suites from single volcanoes are plotted they define clear trends of decreasing Dy/Yb and Dy/Dy* with differentiation, roughly orthogonal to the general depletion–enrichment trend. The trends for single arc volcanoes are interpreted as most probably reflecting an amphibole control, consistent with the concomitant decreases in Ti/Ti* and increasing SiO_2. Available distribution coefficients are, however, also permissive of cpx control on arc REE patterns. Estimated compositions of the continental crust fall along these same trends. In contrast, ocean island basalt (OIB) data all fall to high Dy/Yb, suggesting a significant control by garnet. A global consideration of the data suggests that (1) arc magmas are derived from variably depleted asthenospheric (mid-ocean ridge basalt) mantle sources, (2) arc magma (and continental crust) differentiation is controlled by a mineral phase (or phases) that preferentially partitions MREE and (3) OIB genesis appears to always involve garnet control. We propose that Dy/Dy* is potentially a powerful tool for representing the shapes of REE patterns, especially for large datasets. We also note the importance of using cogenetic rock suites to identify petrogenetic processes rather than regional suites.*

KEY WORDS: *amphibole; differentiation; geochemistry; partition coefficient; REE*

INTRODUCTION—THE USE OF REE PATTERNS

Rare earth element (REE) patterns are widely used as a diagnostic tool in geochemistry. The principles of REE distributions are the same as those for other trace elements in silicate systems. The REE, however, form a coherent group of trace elements owing to their position in the periodic table (the lanthanides). The sizes of REE cations decrease systematically with increasing atomic number from La to Lu. This is known as the lanthanide contraction and it corresponds to progressive filling of an inner electron shell rather than the outer valence shell, which principally dictates geochemical properties. REE cations are normally 3+, although varying oxidation states can result in Eu and Ce occurring naturally in 2+ and 4+ states respectively. The partitioning behaviours of 3+ REE cations vary smoothly from La to Lu, reflecting the small and systematic changes in ionic radius.

*Corresponding author. Telephone: +44 191 334 2300. Fax: +44 191 334 2301. E-mail: j.p.davidson@durham.ac.uk

Typically the use of REE patterns relies on normalization of concentrations (to account for the Oddo–Harkins effect of odd versus even atomic number nuclides) and plotting the pattern as a log concentration versus atomic number. The normalization factor used may vary with the purpose of the investigation, and is not critical provided it is specified. Investigations of crustal rocks and sediments may, for instance, normalize to upper continental crust, whereas studies of oceanic basalts may normalize to mid-ocean ridge basalt (MORB). One of the most widely used normalization schemes is to chondritic abundances [throughout this paper, we use modified chondritic normalizing values of Nakamura (1974) as reported by Kelley *et al.* (2003)]. This scheme has the advantage that the Bulk Earth is believed to have a largely chondritic composition with respect to the REE. Bulk Earth therefore appears on a chondrite-normalized REE plot as a straight line at $C_N = 1$.

The along-group systematic variation in ionic radius of the REE means that distribution coefficients, which are sensitive to the charge and size of an ion in a specific crystal lattice site (Blundy & Wood, 1994), will similarly vary systematically. Thus, processes such as partial melting and fractional crystallization fractionate REE patterns according to the distribution coefficients and abundances of the minerals involved. A great deal of work has accumulated to characterize REE partition coefficients among the minerals involved in petrogenetic processes, and the relative changes in partition coefficients among the REE are better constrained than among other element groups (large ion lithophile elements, high field strength elements, etc.) simply because of the systematic change in elemental properties across the lanthanides. The result is that REE patterns can be interpreted rapidly and simply by visual inspection. A chondrite-normalized MORB pattern, for instance, is characterized by relative light rare earth element (LREE) depletion, which can be interpreted as due to melting of a source from which melt has been previously removed, because the LREE preferentially partition into melts of peridotite with residual olivine and pyroxene. Steep REE patterns with heavy rare earth element (HREE) depletion are commonly interpreted as reflecting garnet control—either by fractional crystallization or residual in a melting source.

The use of a log scale, and the tendency to plot multiple patterns together, can obscure important information that the REE can potentially provide on petrogenetic processes. Figure la illustrates REE data from a suite of cogenetic volcanic rocks from Ijen Volcano, Indonesia (Handley *et al.*, 2007). The patterns are all characterized by a concave-up shape and are apparently sub-parallel. The concave-up pattern would typically be interpreted as an amphibole control inherited from the source or primitive magma, reflecting the preference that amphibole has for middle rare earth elements (MREE) over HREE and LREE. The parallelism of the patterns suggests that the REE have similar bulk distribution coefficients during subsequent differentiation, and the correlation between REE absolute abundance and SiO_2 suggests that all the REE are incompatible (i.e. increase with SiO_2). Indeed, modelling of the REE using a phase with uniformly low $\bar{K}d_{(REE)}$, such as olivine, is apparently capable of reproducing the sub-parallel REE patterns of the differentiates. If, however, we examine the REE data in a different way, by

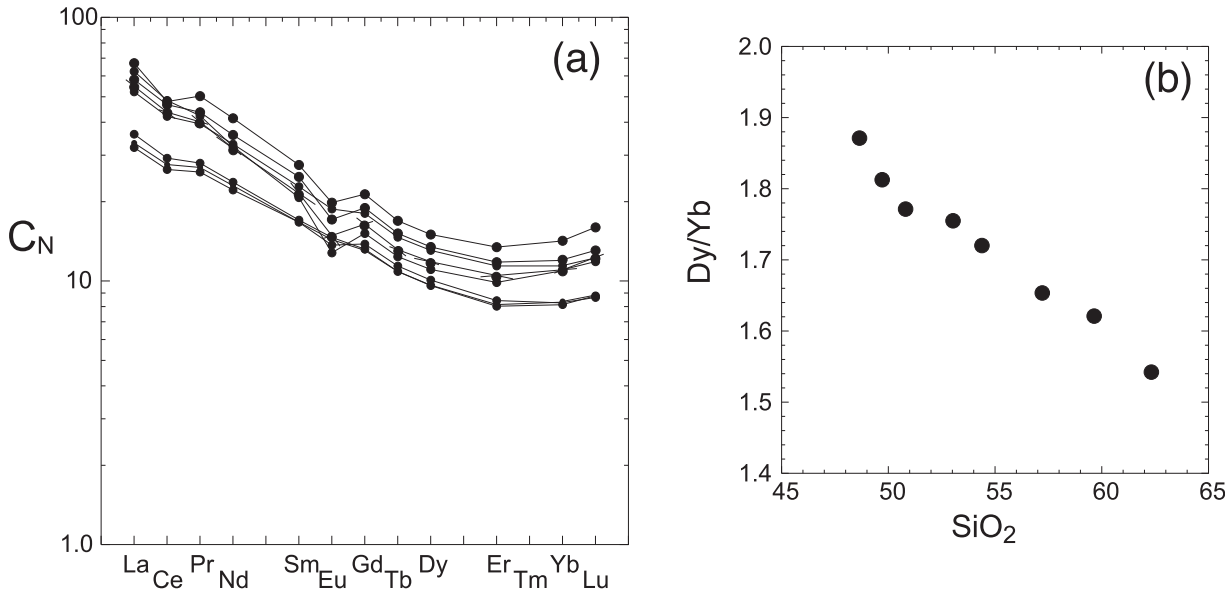

Fig. 1. (a) Chondrite-normalized REE patterns for a cogenetic suite of volcanic rocks from Ijen Volcano, Indonesia (from Handley *et al.*, 2007). (b) Dy/Yb–SiO_2 for the same suite of rocks.

constructing a binary plot of Dy/Yb (representing the MREE/HREE ratio) against SiO_2, a strong correlation is seen (Fig. 1b). In fact, the REE are significantly fractionated during differentiation; a conclusion that is far from obvious through basic inspection of the REE patterns.

EXTRACTING ADDITIONAL MEANING FROM REE PATTERNS; DY/DY*

The key to interpretation of REE patterns is their shape. Many researchers have used proxies for shape such as La/Yb to represent the overall relative LREE enrichment versus HREE depletion and plots of La/Yb versus Dy/Yb have been used to constrain both the extent of melting and the amount of residual garnet (e.g. Rogers *et al.*, 2006). Neither the La/Yb or Dy/Yb ratio, however, gives any sense of curvature for the REE pattern. The sense of curvature, concave up versus concave down, or even not curved at all, is very sensitive to mineralogical control. Both garnet and amphibole partition REE such that La/Yb increases, but the preferences of amphibole and garnet for MREE and HREE respectively mean that amphibole ± clinopyroxene (see below) fractionation will result in greater degrees of curvature. Some researchers have used Dy/Yb ratios as a means for specifically monitoring MREE/HREE fractionation as a proxy for REE pattern curvature (e.g. Davidson *et al.*, 2007).

We propose here a simple proxy for REE curvature, which we refer to as Dy/Dy*. The principle of Dy/Dy*, illustrated in Fig. 2, is similar to the way the Eu anomaly (Eu/Eu*) is constructed. The Eu anomaly is defined by interpolating between the neighboring REE (Sm and Gd) and comparing the observed Eu value with the Eu value obtained by interpolation. Positive Eu/Eu* is an upward spike, negative Eu/Eu* is downward. The Eu anomaly is particularly used to identify partitioning involving plagioclase, which preferentially incorporates Eu when it is in its 2+ form and can substitute effectively for Ca. Dy/Dy* is defined by interpolation between the LREE and HREE (represented by La and Yb respectively) and comparing the interpolated value with the observed one. It is calculated as

$$\frac{\mathrm{Dy}}{\mathrm{Dy}*} = \frac{\mathrm{Dy_N}}{\mathrm{La_N^{4/13}Yb_N^{9/13}}} \quad (1)$$

where Dy_N, La_N, and Yb_N are the chondrite-normalized values of Dy, La and Yb respectively. The normalization constants we use are from Nakamura (1974), but the choice of values makes little difference to the arguments and the distribution of data in the diagrams we present.

The use of Dy/Dy* as a measure of the curvature of the REE pattern can then be combined with a measure of its

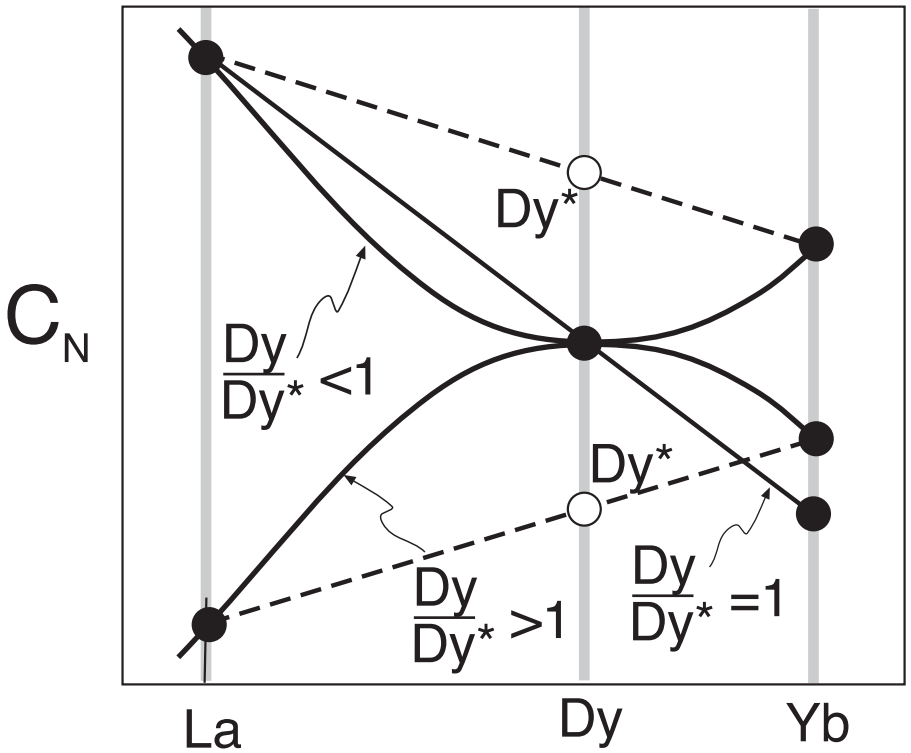

Fig. 2. Principles of construction of the parameter Dy/Dy*. (See text for calculation method.)

gradient (Dy/Yb) such that any REE pattern can be defined as a unique point on a plot of Dy/Dy* vs Dy/Yb. This plot is shown in Fig. 3. Dy/Yb is preferred over La/Yb as a measure of slope as it allows better resolution of REE pattern shape. La/Yb is dominated by the LREE behavior, whereas, as we will show below, it is the slope of the middle-to-heavy REE that allows distinction of mineral controls (Fig. 4). Garnet and amphibole control, for instance, both increase La/Yb, but garnet increases Dy/Yb whereas amphibole decreases this ratio. It should be noted that from equation (1), for a given Dy/Yb and Dy/Dy*, La/Yb is effectively fixed, as demonstrated by the contours drawn in Fig. 3. Equally, it is possible to simply plot La/Yb against Dy/Yb to gain a sense of Dy/Dy*, but we note that the data on such a plot are more dispersed and we feel that having a plotted value to represent REE pattern curvature is more helpful.

The use of a binary diagram means that we can compare large datasets, which is difficult to do with REE patterns, particularly where there is crossing and overlap. Figure 3 can be conveniently divided into quadrants, as illustrated by the schematic inset REE patterns; the upper left

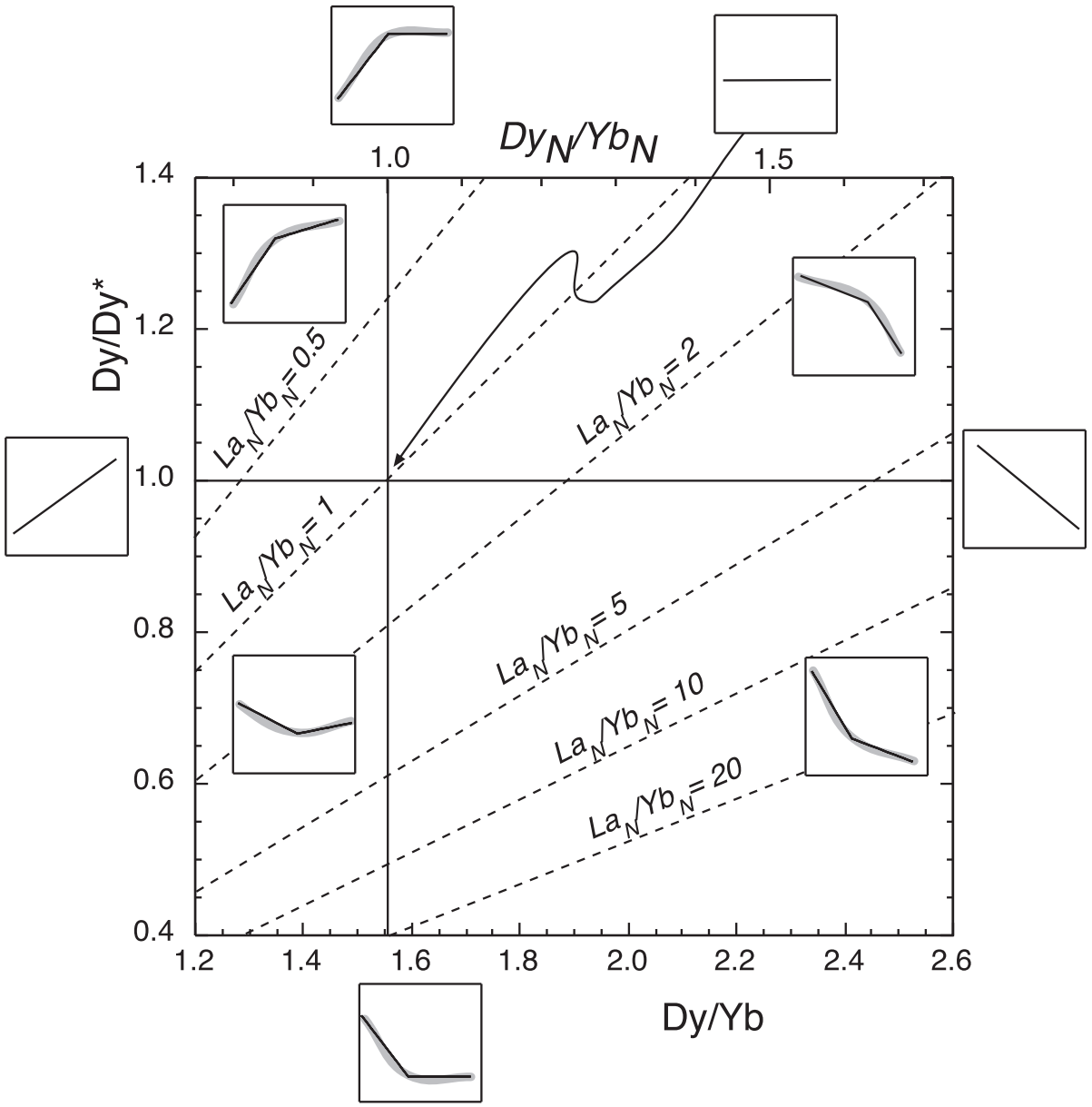

Fig. 3. Dy/Dy*–Dy/Yb as a means for effectively representing a REE pattern as a single point. Sketch REE patterns are shown. In reality these will of course be smoother, as shown by the thick grey lines, but the characterization as two segments allows appreciation of the influence of Dy/Yb and Dy/Dy* on the REE patterns. Contours of La_N/Yb_N are superimposed. N=chondrite-normalized value.

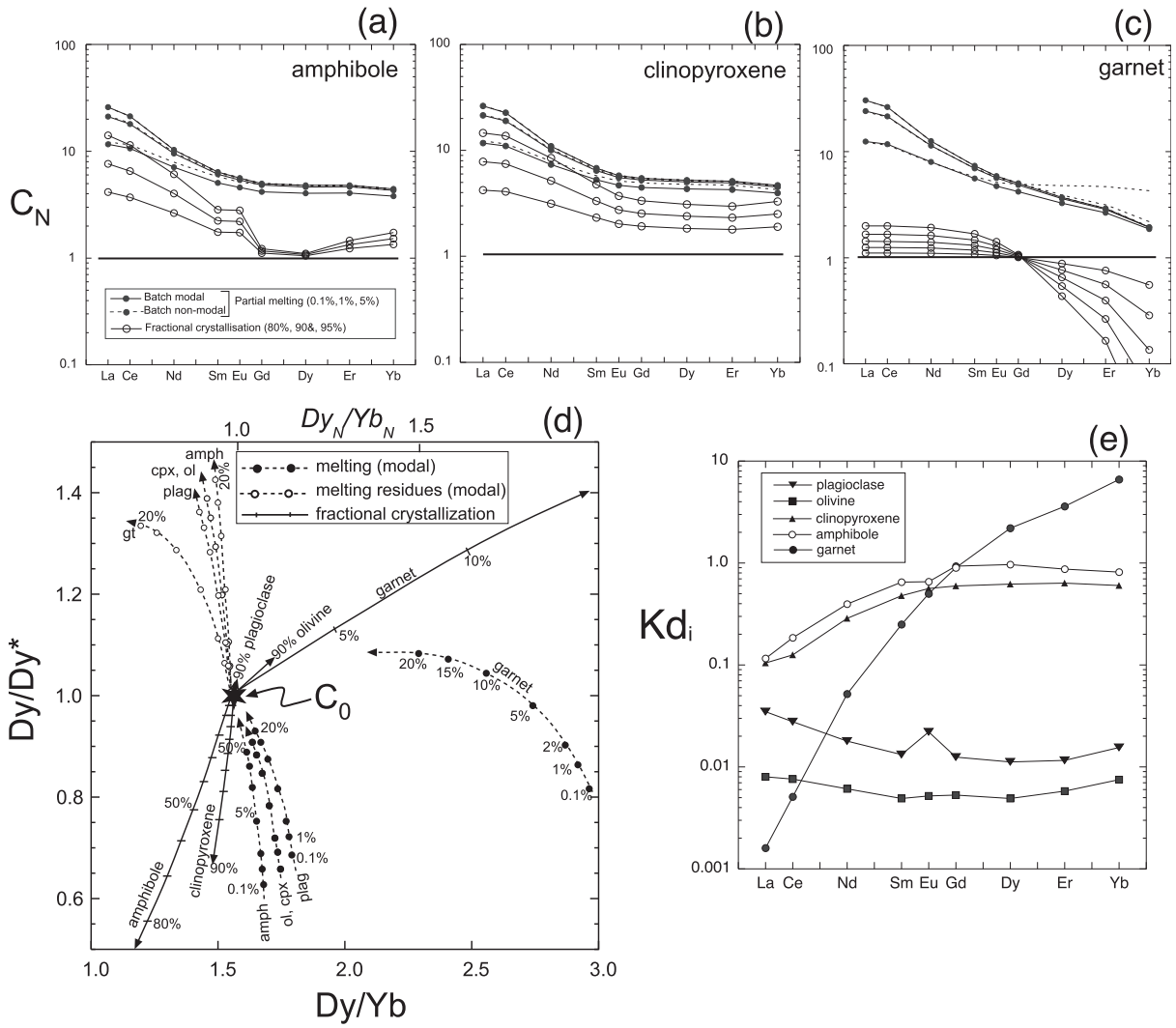

Fig. 4. Schematic effects of mineral controls on REE patterns, starting from a chondritic liquid or solid: (a–c) REE patterns for melting and fractional crystallization shown for amphibole (a), clinopyroxene (b) and garnet (c). Effects are shown for variable degrees of fractional crystallization of each mineral (80%, 90% and 95% crystallization), or degrees of partial melting (0·1%, 1% and 5%) either modal (where bulk D_i is calculated using the modal abundances of the minerals) or non-modal (where D_i is as for modal melting and P_i, representing the proportion in which mineral phases enter the melt, is taken as simply the Kd of the single mineral indicated; i.e. 100% amphibole, clinopyroxene or garnet respectively). It should be noted that modal vs non-modal melting is not significantly different (except in the case of garnet when the HREE are not sequestered as strongly into the residue if garnet is the only phase melting; $P_{i[garnet]} = 1$). Source mineral composition is 0·7 olivine, 0·3 clinopyroxene or 0·7 olivine, 0·25 clinopyroxene, 0·05X where X is amphibole or garnet respectively. It should be noted that the effects of plagioclase and olivine, for which Kd$_{REE}$ are all <0·1, are considered unimportant in fractionating REE. (d) Dy/Dy* vs Dy/Yb showing effects of fractional crystallization and modal partial melting respectively, starting as in (a)–(c) from a chondritic melt or source (C_0). As explained in the text, neither modes nor starting compositions nor phase relations are intended to represent reality, but the general effects on Dy/Dy* and Dy/Yb are robust. (e) Indicative distribution coefficients for major silicate minerals used in models from (a)–(d); from Fujimaki *et al.* (1984), Johnson (1994) and Botazzi *et al.* (1999). Values are interpolated where not listed. (See GERM website; http://earthref.org/GERM/index.html.)

represents LREE-depleted concave-down patterns, such as those that characterize MORB. The lower right quadrant is steep, LREE-enriched/HREE-depleted and concave up, as seen in ocean island basalt (OIB), whereas the lower left quadrant is concave up but with a depletion maximum at the MREE (Dy). The upper right quadrant turns out to be sparsely populated, and represents LREE-enriched concave-down patterns.

MINERAL CONTROL ON REE PARTITIONING

The smooth and systematic variation in partition coefficients consequent on the variation in 'fit' of the REE cations to a given mineral lattice site means that REE patterns are an effective and widely-used means of evaluating control by different minerals. REE partition coefficients (Kd$_{(REE)}$) in a given mineral type are not fixed

because of solid solution variations in the mineral composition, as will be appreciated from a cursory inspection of the GERM partition coefficients database (http://earthref.org/GERM). However, they can be generalized confidently for the main mineral phases that control the compositions of basaltic melts and their differentiates. Figure 4 shows the effects of simple fractional crystallization and batch melting processes from a chondritic starting pattern. This starting composition is clearly not a natural melt, and few natural systems would evolve significantly through a single mineral control. Nevertheless, the contrasting effects of different minerals in controlling REE patterns, such as garnet versus amphibole and clinopyroxene, are clear. Thus, control by garnet (residual in source or fractionated from melt) will rotate REE patterns to enrich LREE and deplete HREE, control by plagioclase (not shown) will enrich all REE but deplete Eu, and control by amphibole or clinopyroxene will lead to concave-up REE patterns by fractionating MREE over HREE and LREE.

The consequences of such mineral controls are illustrated on the Dy/Dy*–Dy/Yb diagram in Fig. 4d. Mineral controls here are represented as vectors rather than changes in pattern. The effects of single mineral controls on batch partial melting and fractional crystallization are clearer in some regards than in Fig. 4a–c. For fractional crystallization both olivine and plagioclase have limited effects on Dy/Yb, or Dy/Dy* unless the degree of crystallization is high (>95%). Amphibole and clinopyroxene are the only major minerals capable of significantly decreasing Dy/Dy* (i.e. increasing the upward concavity of the REE pattern), but amphibole has greater leverage, and correspondingly leads to decreasing Dy/Yb, whereas clinopyroxene has less effect on Dy/Yb. During melting the effect of the bulk distribution coefficient is to buffer the fractionation capacities of single minerals. Nevertheless, it is still amphibole and clinopyroxene that control the capacity to significantly decrease Dy/Dy*. Garnet may reduce or increase Dy/Dy*, but the involvement of garnet drastically increases Dy/Yb regardless of whether the process is melting or crystallization.

USING DY/DY* TO CONSTRAIN SOURCES AND PROCESSES

An appreciation of the shapes of REE patterns that can be derived from Fig. 3, along with the processes by which the REE patterns can be controlled from the models illustrated in Fig. 4, allows us to use the diagram to constrain sources and petrogenetic processes (Fig. 5). Our understanding of mantle sources and melt extraction processes derives largely from the analysis of young oceanic volcanic rocks. The REE patterns of these rocks are affected by three principal controls: (1) the REE pattern of the mantle source; (2) the melting and melt extraction process, in particular the mineral controls discussed above; (3) processes of subsequent differentiation involving the potential mineral controls modelled in Fig. 4, magma mixing, contamination and so on. Extensive differentiation may involve significant control of REE patterns by accessory minerals such as zircon and apatite. These will be interesting to explore in Dy/Dy*–Dy/Yb space, but are not the subject of the current contribution.

Distinguishing source from process is challenging. In a sense the distinction is subtle given that the ultimate control is always mineralogical. Source compositions are dictated by the mineral-controlled processes by which melts have been added or subtracted. Nd isotope data may help in this regard, in that if the mineral fractionation occurred in the past to generate a given source composition (dictating Sm/Nd) then the fractionation will correlate with $^{143}Nd/^{144}Nd$.

Figure 5 shows mantle end-member compositions, along with continental crust, and fields for MORB and OIB data. Normal (N)-MORB data plot, as predicted from the basis on which the diagram was constructed (Fig. 3), in the top left quadrant. MORB data form a negatively sloped array consistent with variable extents of enrichment from a LREE-depleted N-MORB towards enriched (E)-MORB. The MORB array is presumably a long-term source composition effect. Dy/Dy* correlates positively with $^{143}Nd/^{144}Nd$ (at least for samples with both REE and isotope data such as the East Pacific Rise), suggesting that the REE patterns (higher Dy/Dy* = higher Sm/Nd, leading with time to higher $^{143}Nd/^{144}Nd$) have been incubated for long timescales and have not been significantly modified by the more recent melting process from which MORB originated.

OIB, on the other hand, plot in the bottom right-hand quadrant, but typically far to the right of the MORB control array. This observation suggests that OIB are influenced by garnet fractionation (Fig. 4). This is more likely to reflect garnet in deep residual sources than any long-term compositional effect, as we have found no global correlations between $^{143}Nd/^{144}Nd$ and Dy/Yb or Dy/Dy*. Higher degrees of shallower melting of spinel lherzolite at arcs and mid-ocean ridges will tend to minimize any fractionation during melting, whereas lower degrees of garnet lherzolite melting at ocean islands will lead to the melting process significantly modifying source REE characteristics.

Continental crust (except lower crust) has both low Dy/Dy* and low Dy/Yb, and plots far from the bottom right end of the MORB array (Fig. 5). As we will see below, this overlaps with the fields of arc magmas, consistent with the long-held view that sources and processes at subduction zones play an important role in generating the continental crust (Taylor & White, 1965).

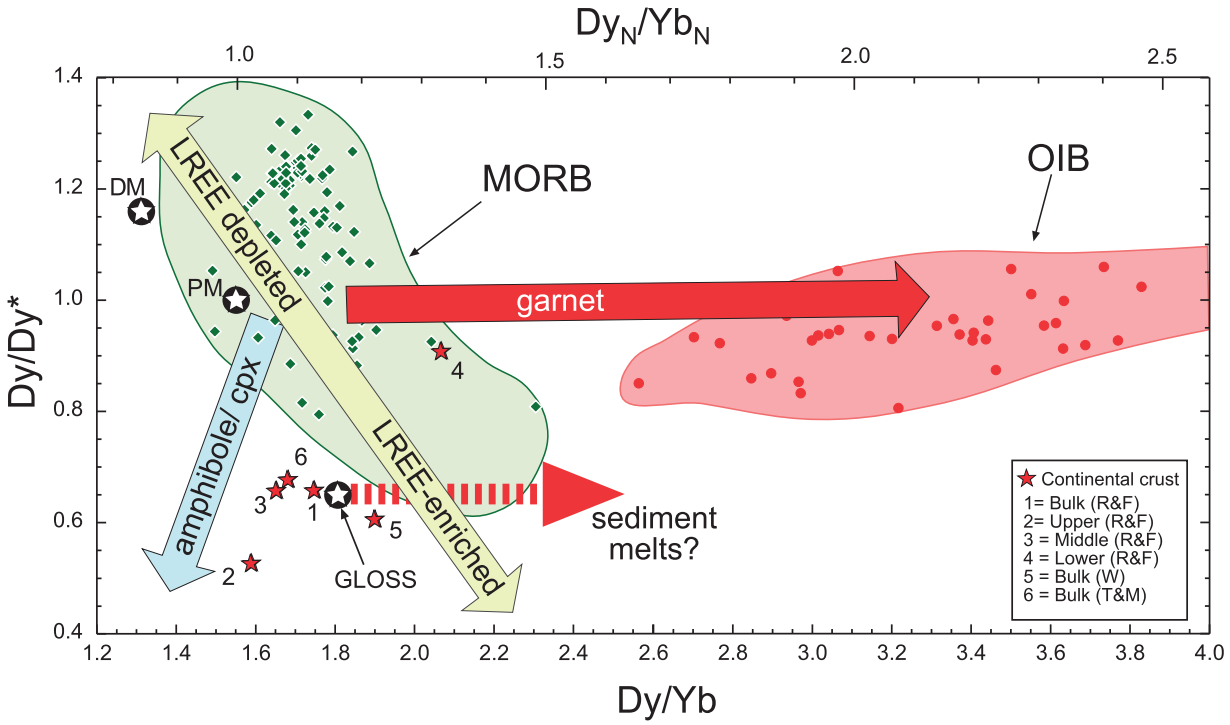

Fig. 5. Plot of Dy/Dy* vs Dy/Yb with extended Dy/Yb scale to show fields for MORB and OIB. OIB field extends to much higher Dy/Yb (Samoa Dy/Yb is up to ~12) reflecting the role of residual garnet. OIB field includes data from Hawaii (Sims *et al.*, 1995, 1999) and the Azores (Beier *et al.*, 2010). MORB field includes N-MORB and E-MORB data from the East Pacific Rise (Niu *et al.*, 1999; Regelous *et al.*, 1999; Turner *et al.*, 2011). PM, primitive mantle (Sun & McDonough, 1989); DM, depleted mantle (Salters & Stracke, 2004); GLOSS, average global subducting sediment (Plank & Langmuir, 1998). Continental crust estimates: R&F, Rudnick & Fountain (1995); W, Wedepohl (1995); T&M, Taylor & McLennan (1985). Vectors for mineral control and melting are indicative, based on general conclusions drawn from modelling in Fig. 4 (garnet increases Dy/Yb over limited increase or decreases in Dy/Dy*, amphibole and clinopyroxene decrease Dy/Dy*, and decrease Dy/Yb depending on the exact choice of *K*d. Sediment melt vector is based on presumed residual garnet (see Hermann & Rubatto, 2009).

REE CHARACTERIZATION OF ARC MAGMAS

We now apply this treatment of REE patterns to our new arc datasets to explore whether more petrogenetic information can be extracted from them. A number of along-arc datasets that include U-series analyses (Turner *et al.*, 1996, 1997, 1998, 1999, 2003; Turner & Foden, 2001; McDermott *et al.*, 2005) were selected for scrutiny. However, most of the trace element data in those studies were produced by a combination of X-ray fluorescence and instrumental neutron activation analysis methods and consequently they are lacking Pb and full REE concentration data. In light of this and the greater accuracy provided by newer techniques, we have re-analysed all of those samples by inductively coupled plasma mass spectrometry (ICP-MS) to provide an internally consistent, high-precision trace element dataset. The concentrations of 36 trace elements were determined on a total of 143 arc lava samples by solution ICP-MS at Boston University using the methods and standards reported by Kelley *et al.* (2003). All sample solutions were measured twice, with an average precision <3% RSD for all the REE. These data and analyses of the international rock standard JA-2 are given in Supplementary Data Table 1 and supersede the earlier data quoted in the referenced papers. The REE data from Supplementary Data Table 1 are plotted in Fig. 6.

Inspection of the REE patterns (Fig. 6) highlights some general distinctions among the arcs studied. The Tonga–Kermadec samples exhibit characteristically flat patterns, relatively depleted in all REE. The Philippines and Indonesia samples, in contrast, are enriched in most REE with generally sloping patterns (LREE>HREE). The Lesser Antilles samples show perhaps the greatest diversity, with variable degrees of LREE enrichment from nearly flat to highly LREE enriched. Kamchatka and Vanuatu samples are all moderately LREE enriched.

When the samples are plotted on a Dy/Dy*–Dy/Yb diagram these characteristics are arguably better appreciated (Fig. 7a). The arcs appear as a series of irregular fields that step down along the negative 'control' trend (MORB) of Fig. 5, with the most depleted arcs to the top left (Tonga–Kermadec) and more enriched to the bottom right (Indonesia). The 'stepping down' of the arc fields along the MORB trend might be due to variable incorporation of sediment, increasing towards higher Dy/Yb

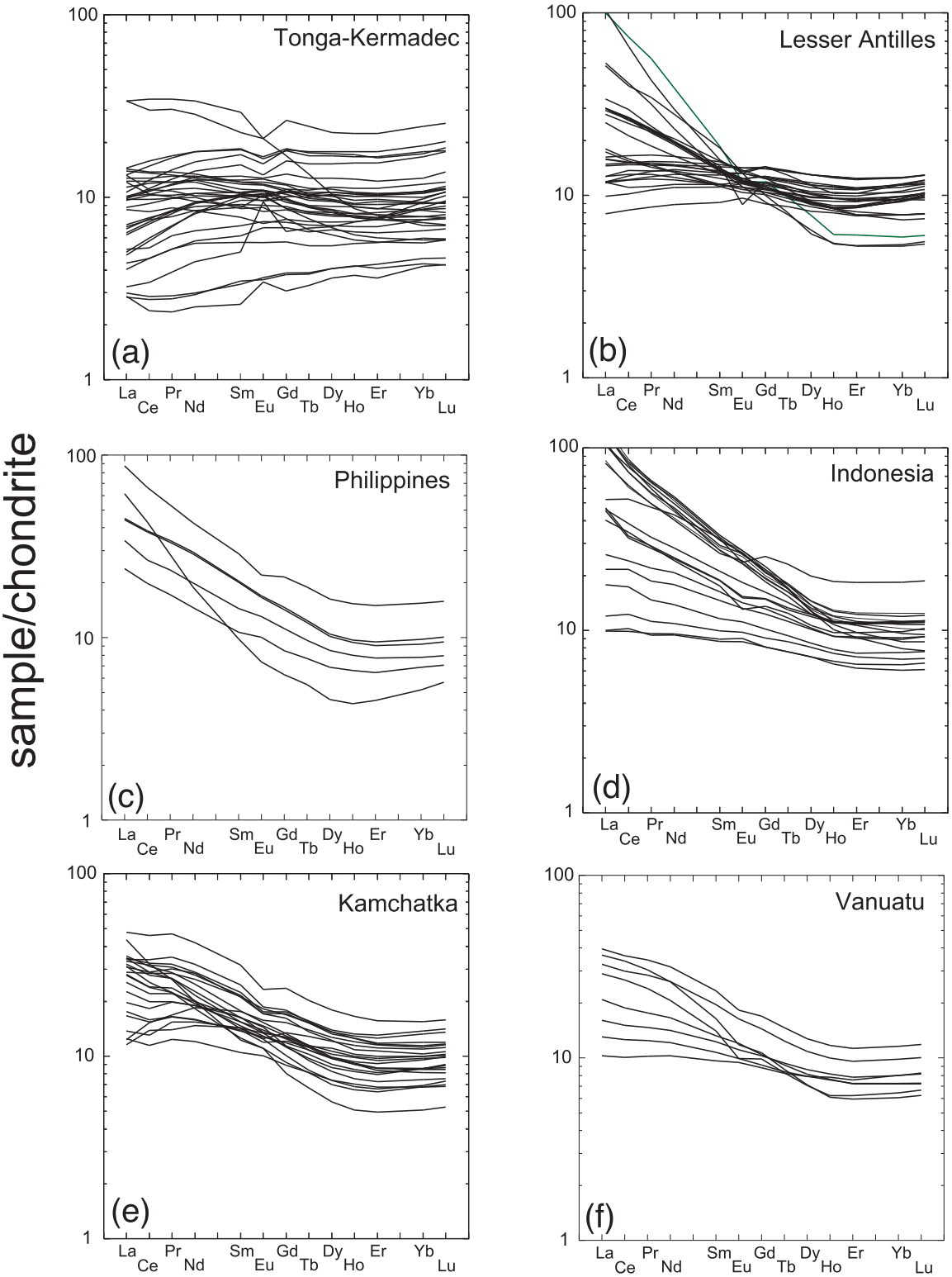

Fig. 6. REE patterns for young volcanic rocks from arcs: (a) Tonga–Kermadec; (b) Lesser Antilles; (c) Philippines; (d) Indonesia; (e) Kamchatka; (f) Vanuatu. Data from Supplementary Data Table 1.

and lower Dy/Dy* (Fig. 5). If so, it would suggest that the amount of sediment in the arc sources increases progressively from Tonga-Kermadec through to The Philippines.

If we re-plot this figure using suites of data from single volcanoes, which clearly define differentiation trends (as used by Davidson *et al.*, 2007), then some convincing general trends appear. Superimposed on the general arc characteristics of depletion versus enrichment (Fig. 7a) are clear trends of correlated decreasing Dy/Dy* and decreasing Dy/Yb (Fig. 7b). These trends also correlate with increasing SiO_2, as shown by Davidson *et al.* (2007), consistent with intracrustal differentiation processes. An exception to the positive trends defined by most cogenetic arc volcano suites are the Cotopaxi data, which form a trend at considerably higher Dy/Yb than the rest of the arc data. The Cotopaxi REE data in Fig. 7b are consistent with the involvement of garnet during differentiation in the thick northern Andean crust, as deduced independently on the basis of other geochemical characteristics (Garrison *et al.*, 2011).

We can now re-explore the interpretation of the arc fields in Fig. 7a as reflecting variable sediment additions to a MORB-like mantle source. With the better-resolved trends of Fig. 7b we can back-project towards putative primitive or primary compositions (large symbols in Fig. 7b). Now we see that it is only the most differentiated members of a given volcanic suite that overlap with crustal averages, which suggests either that primitive arc magmas differentiate towards continental crust-like compositions, or that they mix with it during differentiation. The primitive arc magmas, which lie along the high Dy/Yb side of the MORB trend, are difficult to reproduce by source mixing between MORB sources and average sediment. As discussed below, however, arc sources might be generated by mixing between MORB mantle and sediment melts that lie to higher Dy/Yb (Fig. 5).

The differentiation trends, which progress from the control trend towards the bottom left-hand corner of the diagram (Fig. 7), are consistent with the claim of Davidson *et al.* (2007) that amphibole has an important influence. The controls illustrated in Fig. 4, however, suggest that clinopyroxene may arguably also (or alternatively) play a role in controlling arc differentiation trends. Although the example Kd values we have chosen for cpx do not significantly decrease Dy/Yb with differentiation, this may simply be due to an inappropriate choice of values. Blundy *et al.* (1998), for instance, reported pressure dependence of REE distribution coefficients for cpx.

A trawl of the GERM database yields D_{Dy}/D_{Yb} (cpx) varying between 0·72 and 1·38 (average = 1·09, $n = 23$) over a spectrum of rock compositions from peridotite

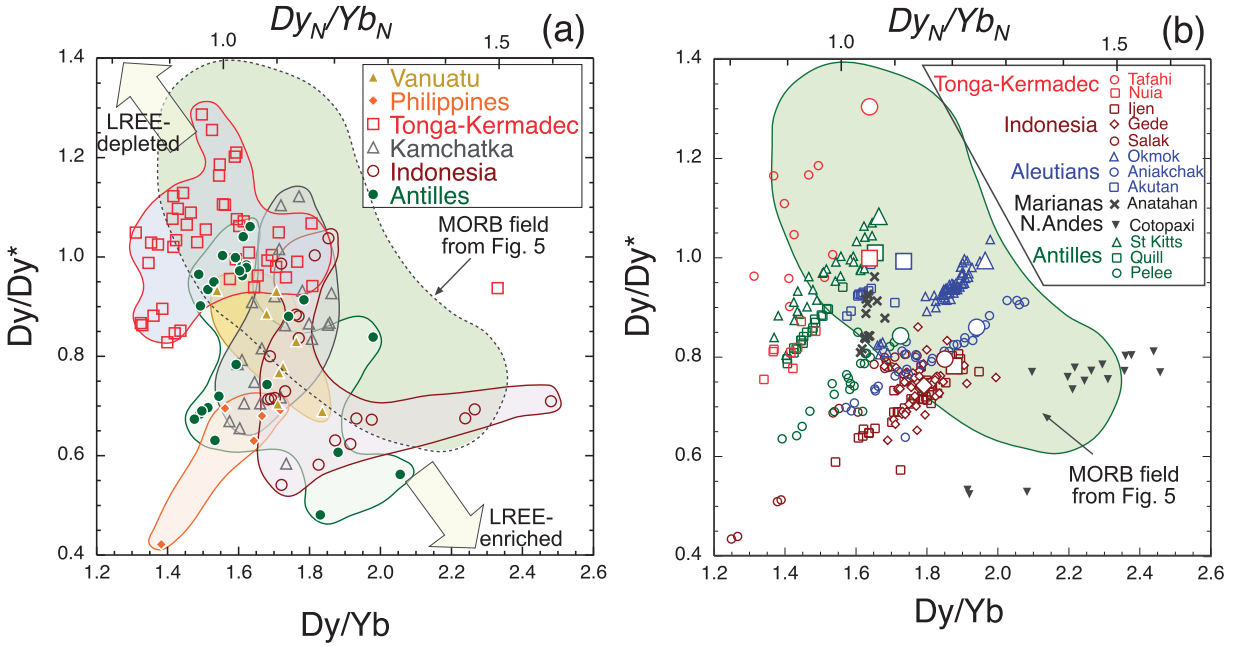

Fig. 7. (a) Data from Fig. 6 plotted as Dy/Dy* vs Dy/Yb, showing very general differences among arcs, with all the data forming a broad array interpreted to represent variable degrees of source LREE depletion (top left) to LREE enrichment (bottom right). (b) Same diagram but with data from single volcanoes, showing distinct trends for many. Data sources: Tonga–Kermadec from Acland (1996), Aleutians from Finney *et al.* (2008) (Okmok) and George *et al.* (2004) (Aniakchak and Akutan); Lesser Antilles from Toothill *et al.* (2007) (Mt Misery on St Kitts) and Davidson & Wilson (2011) (Mt Pelée, Martinique; The Quill, Statia); Northern Andes (Cotopaxi) from Garrison *et al.* (2011). Indonesia from Handley *et al.* (2007) (Ijen), Handley *et al.* (2008) (Salak) and Handley *et al.* (2009) (Gede); Marianas (Anatahan) from Wade *et al.* (2005). Large symbols towards the high Dy/Dy* ends of trends (where trends are clearly defined) correspond to primitive magma (mantle melt) values determined by regression of Dy/Yb vs SiO_2 to 48% SiO_2.

to rhyolite, so clinopyroxene may decrease or increase Dy/Yb with differentiation. For amphibole, Dy/Yb universally decreases with fractionation; D_{Dy}/D_{Yb} (amph) varies between 1·32 and 2·35 (average = 1·66, $n = 10$) over the spectrum of rock (and therefore amphibole) compositions from peridotite to rhyolite. Furthermore, as pointed out by Davidson *et al.* (2007), clinopyroxene alone has no leverage on primitive melt SiO_2 contents (the SiO_2 content of cpx is around 45–50%, similar to primitive basalts), whereas amphibole with $SiO_2 < 40\%$ is better able to increase SiO_2 in differentiates, as seen at arc suites.

Although it is not our primary objective to concentrate on the role of amphibole fractionation in arc lavas here, Fig. 8 shows that there is a strong positive correlation between Dy/Dy* and Ti/Ti* even when only the along-arc dataset of Supplementary Data Table 1 is plotted. Ti/Ti* provides a measure of the size of the (generally negative) Ti anomaly in mantle-normalized trace element patterns and, because arc lavas can exhibit both Zr–Hf and Eu anomalies, we define this as

$$\frac{\mathrm{Ti}}{\mathrm{Ti}*} = \frac{\frac{\mathrm{Ti}}{\mathrm{Ti_{PM}}}}{\frac{\left(\frac{\mathrm{Sm}}{\mathrm{Sm_{PM}}} + \frac{\mathrm{Gd}}{\mathrm{Gd_{PM}}}\right)}{2} + \frac{\left(\frac{\mathrm{Tb}}{\mathrm{Tb_{PM}}}\right)}{2}} \qquad (2)$$

where the subscript PM refers to the primitive mantle values of Sun & McDonough (1989). According to the GERM database, the basalt/andesite partition coefficients for Ti in amphibole range from 0·48 to 7·96 whereas those for clinopyroxene are far lower, ranging from 0·09 to 0·89. Moreover, for any single and internally consistent dataset, Ti is significantly (2–10 times) more compatible in amphibole than in clinopyroxene (e.g. Adam & Green, 2011). This provides support for the notion that the decreases in Dy/Dy* reflect amphibole fractionation. Of course, other mineral phases, such as magnetite, may contribute as

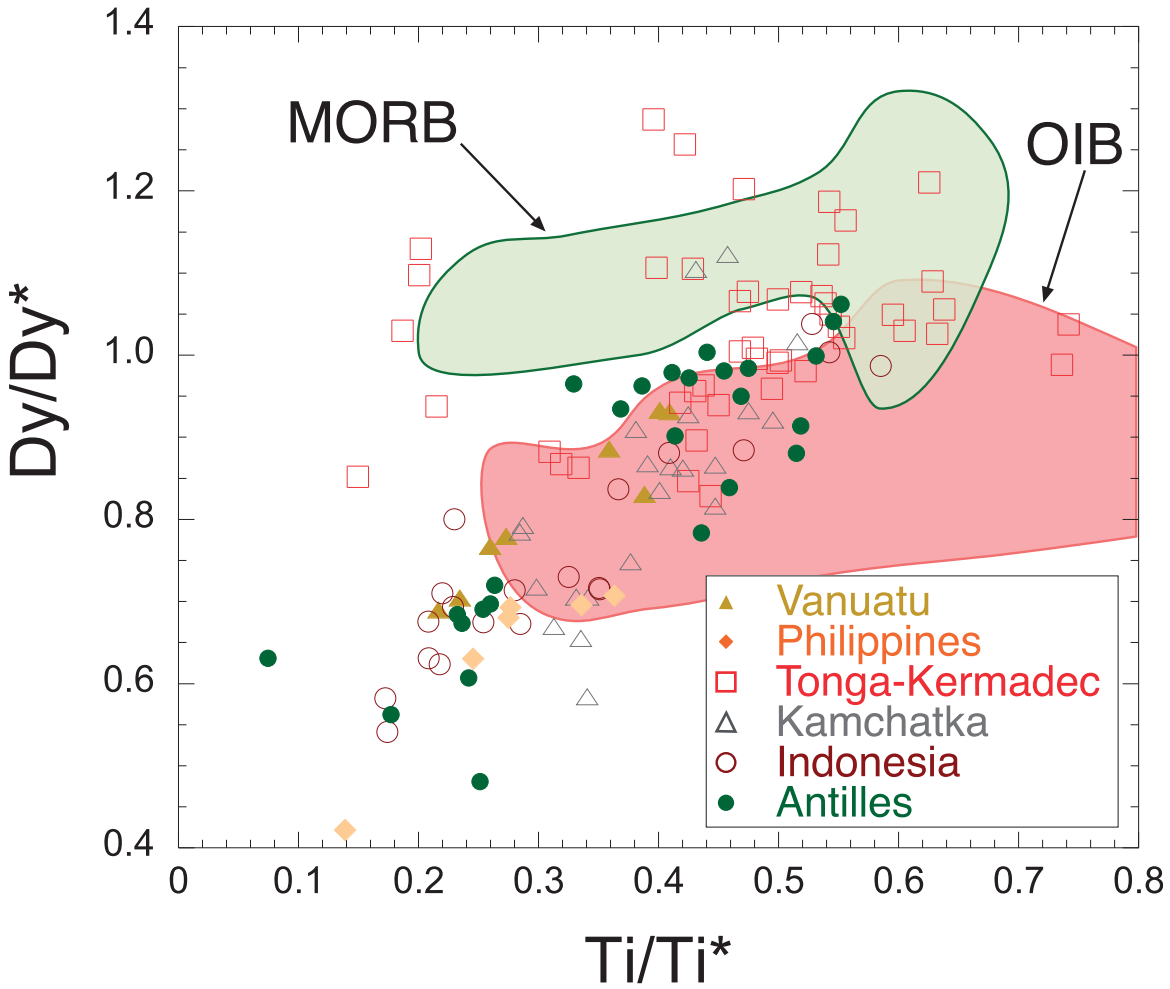

Fig. 8. Plot of Dy/Dy* vs Ti/Ti* showing the along-arc data suites from Supplementary Data Table 1.

much or more to the development of the negative Ti anomaly with arc magma differentiation. Both amphibole and magnetite are preferentially saturated early in arc magmas that are cool and hydrous (Sisson & Grove, 1993) and so explain the deviation of evolving arc magmas from the MORB trend.

The negative 'control' trend anchoring the right-hand side of the arc arrays in Fig. 7, where primitive arc basalts overlap the MORB field, suggests that arc magmas may be derived from variably depleted or enriched MORB source mantle, rather than from OIB source material as has been suggested by some workers (e.g. Morris & Hart, 1983; Gazel *et al.*, 2009). In effect, arc basalts lying at the high Dy/Dy* end of the differentiation arrays overlap with MORB in defining a negative array from LREE-depleted to LREE-enriched (Fig. 7). This could mean that primary arc magmas inherit their REE characteristics directly from the unmodified mantle wedge. However, Woodhead *et al.* (2001) showed in a study of paired arc–back-arc sources that arc sources are ubiquitously modified by a slab-derived component, even for elements as supposedly fluid-immobile as Hf. Alternatively then, the control trend might be interpreted in terms of mixtures between variably depleted mantle and sediment, as was suggested by Plank (2005) on the basis of Th/La–Sm/La arrays, or more probably sediment melts, which would probably lie to higher Dy/Yb [as shown in Fig. 5 and in the experiments of Hermann & Rubatto (2009)]. A possible test is to see whether the position on the array correlates with Nd isotope ratios, as sediment–mantle mixing would be expected to generate sources with a positive $^{143}Nd/^{144}Nd$–Dy/Dy* correlation. No convincing correlation appears to exist using the data from Fig. 7b, perhaps because sediment compositions vary so widely in their $^{143}Nd/^{144}Nd$ compositions.

Finally, we note that the single volcano data of Fig. 7b are probably not as consistent and high quality as our new data, originating as they do from a variety of different laboratories with no attempt to cross-standardize. On the other hand, the higher quality dataset used in Fig. 7a has few cogenetic suites and is a more random sampling of a larger number of volcanoes along each arc, as the samples were selected on the basis of their young age, which was a prerequisite for U-series analysis. The trends observed in Fig. 7b become apparent only because the selection of cogenetic samples provides for better trend definition. For instance, the broad field of Lesser Antilles data defined in Fig. 7a, which is generally elongate along the control trend (top left to bottom right), should be noted. In Fig. 7b, where three separate Lesser Antilles volcanoes are plotted, each defines a very tight differentiation trend from the control trend towards the bottom left. Even volcanoes separated by less than 20 km along the arc (Mt Misery on St Kitts and The Quill on Statia) define clearly distinct sub-parallel trends. This serves to illustrate an important principle: that the method of sampling (in this case selection of extensive cogenetic suites from a single volcano versus mixed samples from many volcanoes along a given arc) is at least as important as the type and quality of data in our capacity to identify and understand petrogenetic processes from geochemical data.

CONCLUSIONS

We present a new easy-to-calculate parameter, Dy/Dy*, which represents the curvature of REE patterns. In conjunction with another REE parameter, Dy/Yb, we can show the following.

(1) Global MORB data define a broad negative array from LREE-depleted concave-down patterns (N-MORB) to flat or slightly LREE-enriched concave-up patterns (E-MORB).
(2) Global arc data broadly follow this array, with single arcs overlapping with different sections of the MORB array.
(3) Well-constrained data from single arc volcanoes describe differentiation trends within the respective arc fields, which are positive and seem to reflect amphibole, or perhaps clinopyroxene, control (fractionated or residual in crustal melting) such that upward curvature of REE patterns increases and Dy/Yb decreases with differentiation.
(4) Continental crust compositions (bulk crust, lower and upper crust) all plot along arc differentiation trends, consistent with the view that processes at subduction zones exert a strong influence on the composition of the continents.
(5) The distribution of data from MORB, arcs and OIB suggests that arc magmas are derived from variably enriched MORB source mantle with which they overlap. Global OIB data all appear to plot well to the right of the MORB control array, suggesting significant garnet control.
(6) Finally, the use of two complementary arc datasets underscores the need to consider cogenetic suites of samples to constrain petrogenetic processes. In this case, the data from single volcanoes, although arguably of poorer quality than our global dataset, illuminate trends that are not discerned from the latter. This argues that data quality must be accompanied by (and is at least as important as) an appropriate sampling strategy.

ACKNOWLEDGEMENTS

We are grateful to Katie Kelley for her mastery and diligence in helping obtain the ICP-MS analyses, to undergraduates Sarah Burns and Briana Mordick for their careful work in the chemistry lab, and to Boston

University for support of the laboratory. The manuscript benefited from extensive discussions with John Adam, and with the Durham Volc Coffee Group, especially Ed Llewellin and Jeroen van Hunen, who helped with the formulations. Comments from Nick Rogers and an anonymous reviewer helped to improve the paper.

FUNDING

The Faculty of Science (Durham) is thanked for seedcorn funding for J.P.D. to visit S.P.T. and carry out the work. Funding for analyses at Boston University was provided by US NSF grant EAR-0233712.

SUPPLEMENTARY DATA

Supplementary data for this paper are available at *Journal of Petrology* online.

REFERENCES

Acland, S. (1996). Magma genesis in the northern Lau Basin, S.W. Pacific. PhD dissertation, University of Durham.

Adam, J. & Green, T. (2011). Trace element partitioning between mica- and amphibole-bearing garnet lherzolite and hydrous basanitic melt: 2. Tasmanian Cainozoic basalts and the origins of intraplate basaltic magmas. *Contributions to Mineralogy and Petrology* **161**, 883–899.

Beier, C., Turner, S. P., Plank, T. & White, W. (2010). A preliminary assessment of the symmetry of source composition and melting dynamics across the Azores plume. *Geochemistry, Geophysics, Geosystems*, doi:10.1029/2009GC002833.

Blundy, J. D. & Wood, B. J. (1994). Prediction of crystal–melt partition coefficients from elastic moduli. *Nature* **372**, 452–454.

Blundy, J. D., Robinson, J. A. C. & Wood, B. J. (1998). Heavy REE are compatible in clinopyroxene on the spinel lherzolite solidus. *Earth and Planetary Science Letters* **160**, 493–504.

Botazzi, P., Tiepolo, M., Vanucci, R., Zanetti, A., Brumm, R., Foley, S. F. & Oberti, R. (1999). Distinct site preferences for heavy and light REE in amphibole and the prediction of $^{Amph/L}D_{REE}$. *Contributions to Mineralogy and Petrology* **137**, 36–45.

Davidson, J. P. & Wilson, B. M. (2011). Differentiation and source processes at Mt Pelée and the Quill; active volcanoes in the Lesser Antilles Arc. *Journal of Petrology* **52**, 1493–1531, doi:10.1093/petrology/egq095.

Davidson, J., Turner, S., Handley, H., Macpherson, C. & Dosseto, A. (2007). An amphibole 'sponge' in arc crust? *Geology* **35**, 787–790..

Finney, B., Turner, S., Hawkesworth, C., Larson, J., Nye, C., George, R., Bindemann, I. & Eichelberger, J. (2008). Magmatic differentiation at an island-arc caldera: Okmok volcano, Aleutian Islands, Alaska. *Journal of Petrology* **49**, 857–884.

Fujimaki, H., Tatsumoto, M. & Aoki, K. (1984). Partition coefficients of Hf, Zr, and REE between phenocrysts and groundmasses. *Journal of Geophysical Research* **89**, 662–672.

Garrison, J. M., Davidson, J. P., Hall, M. & Mothes, P. (2011). Geochemistry and petrology of the most recent deposits from Cotopaxi Volcano, Northern Volcanic Zone, Ecuador. *Journal of Petrology* **52**, 1641–1678, doi:10.1093/petrology/egr023.

Gazel, E., Carr, M. J., Hoernle, K., Feigenson, M. D., Szymanski, D., Hauff, F. & van den Bogaard, P. (2009). Galapagos-OIB signature in southern Central America: Mantle refertilization by arc–hot spot interaction. *Geochemistry, Geophysics, Geosystems* **10**, Q02S11, doi:10.1029/2008GC002246.

George, R., Turner, S., Hawkesworth, C., Nye, C., Bacon, C., Stelling, P. & Dreher, S. (2004). Chemical versus temporal controls on the evolution of tholeiitic and calc-alkaline magmas at two volcanoes in the Aleutian arc. *Journal of Petrology* **4**, 203–219.

Handley, H. K., Macpherson, C. G., Davidson, J. P., Berlo, K. & Lowry, D. (2007). Constraining fluid and sediment contributions to subduction-related magmatism in Indonesia: Ijen Volcanic Complex, Indonesia. *Journal of Petrology* **48**, 1155–1184.

Handley, H. A., Davidson, J. P., Macpherson, C. G. & Stimac, J. A. (2008). Untangling differentiation in arc lavas: constraints from unusual minor and trace element variations at Salak Volcano, Indonesia. *Chemical Geology* **255**, 360–376.

Handley, H. A., Macpherson, C. G. & Davidson, J. P. (2009). Geochemical and Sr–O isotopic constraints on magmatic differentiation at Gede Volcanic Complex (GVC), West Java, Indonesia. *Contributions to Mineralogy and Petrology* **159**, 885–908.

Hermann, J. & Rubatto, D. (2009). Accessory phase control on the trace element signature of sediment melts in subduction zones. *Chemical Geology* **265**, 512–526.

Johnson, K. T. M. (1994). Experimental cpx/and garnet/melt partitioning of REE and other trace elements at high pressures; petrogenetic implications. *Mineralogical Magazine* **58**, 454–455.

Kelley, K. A., Plank, T., Ludden, J. & Staudigel, H. (2003). Composition of altered oceanic crust at ODP Sites 801 and 1149. *Geochemistry, Geophysics, Geosystems* **4**, doi:10.1029/2002GC000435.

McDermott, F., Delfin, F. G., Defant, M. J., Turner, S. & Maury, R. (2005). The petrogenesis of magmas from Mt. Bulusan and Mayon in the Bicol arc, the Philippines. *Contributions to Mineralogy and Petrology* **150**, 652–670.

Morris, J. D. & Hart, S. R. (1983). Isotopic and incompatible element constraints on the genesis of island arc volcanics from Cold Bay and Amak Island, Aleutians, and implications for mantle structure. *Geochimica et Cosmochimica Acta* **47**, 2015–2030.

Nakamura, N. (1974). Determination of REE, Ba, Fe, Mg, Na and K in carbonaceous and ordinary chondrites. *Geochimica et Cosmochimica Acta* **38**, 757–775.

Niu, Y., Collerson, K. D., Batiza, R., Wendt, J. L. & Regelous, M. (1999). Origin of enriched-type mid-ocean ridge basalt at ridges far from mantle plumes: the East Pacific Rise at 11°20'N. *Journal of Geophysical Research* **104**, 7067–7087.

Plank, T. (2005). Constraints from thorium/lanthanum on sediment recycling at subduction zones and the evolution of the continents. *Journal of Petrology* **46**, 921–944.

Plank, T. & Langmuir, C. H. (1998). The chemical composition of subducting sediment and its consequences for the crust and mantle. *Chemical Geology* **145**, 325–394.

Regelous, M., Niu, Y., Wendt, J. I., Batiza, R., Greig, A. & Collerson., K. D. (1999). Variations in the geochemistry of magmatism on the East Pacific Rise at 10°30'N since 800 ka. *Earth and Planetary Science Letters* **168**, 45–63.

Rogers, N. W., Thomas, L. E., Macdonald, R., Hawkesworth, C. J. & Mokadem, F. (2006). ^{238}U–^{230}Th disequilibrium in recent basalts and dynamic melting beneath the Kenya rift. *Chemical Geology* **234**, 148–168.

Rudnick, R. L. & Fountain, D. M. (1995). Nature and composition of the continental crust: a lower crustal perspective. *Reviews in Geophysics* **33**, 267–309.

Salters, V. J. M. & Stracke, A. (2004). Composition of the depleted mantle. *Geochemistry, Geophysics, Geosystems* **5**, doi:10.1029/2003GC000,597.

Sims, K. W. W., DePaolo, D. J., Murrell, M. T., Baldridge, W. S., Goldstein, S. J. & Clague, D. A. (1995). Mechanisms of magma generation beneath Hawaii and mid-ocean ridges: uranium/thorium and samarium/neodymium isotopic evidence. *Science* **267**, 508–512.

Sims, K. W. W., DePaolo, D. J., Murrell, M. T., Baldridge, W. S., Goldstein, S., Clague, D. & Jull, M. (1999). Porosity of the melting zone and variations in the solid mantle upwelling rate beneath Hawaii: inferences from ^{238}U–^{230}Th–^{226}Ra and ^{235}U–^{231}Pa disequilibria. *Geochimica et Cosmochimica Acta* **63**, 4119–4138.

Sisson, T. W. & Grove, T. L. (1993). Temperatures and H_2O contents of low-MgO high-alumina basalts. *Contributions to Mineralogy and Petrology* **113**, 143–166.

Sun, S-s. & McDonough, W. F. (1989). Chemical and isotopic systematics of oceanic basalts: implications for mantle composition and processes. In: Saunders, A. D. & Norry, M. J. (eds) *Magmatism in the Ocean Basins. Geological Society, London, Special Publications* **42**, 313–345.

Taylor, S. R. & McLennan, S. M. (1985). *The Continental Crust: Its Composition and Evolution.* Oxford: Blackwell.

Taylor, S. R. & White, A. J. R. (1965). Geochemistry of andesites and the growth of continents. *Nature* **208**, 271–273.

Toothill, J., Williams, C. A., Macdonald, R., Turner, S. P., Rogers, N. W., Hawkesworth, C. J., Jerram, D. A., Ottley, C. J. & Tindle, A. G. (2007). A complex petrogenesis for an arc magmatic suite, St Kitts, Lesser Antilles. *Journal of Petrology* **48**, 3–42.

Turner, S. & Foden, J. (2001). U–Th–Ra disequilibria, Sr–Nd–Pb isotope and trace element variations in Sunda arc lavas: predominance of a subducted sediment component. *Contributions to Mineralogy and Petrology* **142**, 43–57.

Turner, S., Hawkesworth, C., Macdonald, R., Black, S. & van Calsteren, P. (1996). U-series isotopes and destructive plate margin magma genesis in the Lesser Antilles. *Earth and Planetary Science Letters* **142**, 191–207.

Turner, S., Hawkesworth, C., Rogers, N., Bartlett, J., Worthington, T., Hergt, J., Pearce, J. & Smith, I. (1997). ^{238}U–^{230}Th disequilibria, magma petrogenesis and flux rates beneath the depleted Tonga–Kermadec island arc. *Geochimica et Cosmochimica Acta* **61**, 4855–4884.

Turner, S., McDermott, F., Hawkesworth, C. & Kepezhinskas, P. (1998). A U-series study of Kamchatka and the Aleutians: constraints on source composition and melting conditions. *Contributions to Mineralogy and Petrology* **133**, 217–234.

Turner, S. P., Peate, D. W., Hawkesworth, C. J., Eggins, S. M. & Crawford, A. J. (1999). Two mantle domains and the time scales of fluid transfer beneath the Vanuatu arc. *Geology* **27**, 963–966.

Turner, S., Foden, J., George, R., Evans, P., Varne, R., Elburg, M. & Jenner, G. (2003). Rates and processes of potassic magma generation at Sangeang Api volcano, east Sunda arc, Indonesia. *Journal of Petrology* **44**, 491–515.

Turner, S., Beier, C., Niu, Y. & Cook, C. (2011). U–Th–Ra disequilibria and the extent of off-axis volcanism arcoss the East Pacific Rise at 9°30'N, 10°30'N and 11°20'N. *Geochemistry, Geophysics, Geosystems*, doi:10.1029/2010GC003403.

Wade, J. A. *et al.* (2005). The May 2003 eruption of Anatahan volcano, Mariana Islands: Geochemical evolution of a silicic island-arc volcano. *Journal of Volcanology and Geothermal Research* **146**, 139–170.

Wedepohl, K. H. (1995). The composition of the continental crust. *Geochimica et Cosmochimica Acta* **59**, 1217–1232.

Woodhead, J. D., Hergt, J. M., Davidson, J. P. & Eggins, S. M. (2001). Hafnium isotope evidence for 'conservative' element mobility during subduction zone processes. *Earth and Planetary Science Letters* **192**, 331–346.